Low-Frequency Resonance Raman Characterization of the Oxygen-Evolving Complex of Photosystem II

Agnes Cua,[†] David H. Stewart,[‡,§] Michael J. Reifler,[‡] Gary W. Brudvig,*[,‡] and David F. Bocian*[,†]

Contribution from the Departments of Chemistry, University of California, Riverside, California 92521-0403, and Yale University, P.O. Box 208107, New Haven, Connecticut 06520-8107

Received September 9, 1999. Revised Manuscript Received November 22, 1999

Abstract: The O_2-evolving complex (OEC) of photosystem II (PSII) contains a tetramanganese (Mn_4) cluster, a redox-active tyrosine, and Ca^{2+}/Cl^- ions, but its molecular structure has not been determined. Vibrational spectroscopy has the potential of providing new structural information for the OEC, particularly the Mn_4 cluster. Toward this goal, the vibrational characteristics of the OEC of PSII were examined using near-infrared (NIR) excitation Raman spectroscopy. NIR excitation decreases the background contribution from chlorophyll emission/Raman scattering and affords the opportunity of probing selectively low-energy electronic transitions of the Mn_4 cluster. The primary emphasis of the Raman study was on the low-frequency range of the spectrum (220−620 cm^{-1}) where Mn−ligand vibrational modes are expected to occur. The low-frequency region was examined for both the S_1 and S_2 oxidation states of the Mn_4 cluster. A particular effort was made to probe a NIR transition of the S_2 state that has been reported to mediate photoconversion from the multiline to the $g = 4.1$ form of the S_2 state [Boussac et al. *Biochemistry* **1996**, *35*, 6984−6989]. The Raman studies revealed the following: (1) the Raman spectra of Mn-depleted PSII and PSII in the S_2 state are nearly identical; (2) the Raman spectrum of PSII in the S_1 state displays several unique low-frequency bands not present in the S_2 state that can be assigned as Mn−ligand vibrational modes and appear to maximize in intensity at $\lambda_{ex} \sim 820$ nm; and (3) several of the S_1 state Raman bands are shifted by D_2O/H_2O exchange. Collectively, these results indicate that the S_1 state of the Mn_4 cluster (1) has a NIR electronic transition from which resonance enhanced Raman scattering can be induced and (2) is coordinated by at least two H_2O or OH^- groups. The studies reported herein also demonstrate the potential of NIR-excitation Raman techniques for probing selectively the OEC in PSII and, in particular, for characterizing the coordination environment of the Mn_4 cluster.

Introduction

Photosystem II (PSII) is a transmembrane protein complex in higher plants, algae, and cyanobacteria that facilitates the conversion of photons into chemical energy by catalyzing light-driven H_2O oxidation and plastoquinone reduction. Light-harvesting pigments in the complex channel energy to a chlorophyll dimer (P680) that initiates photochemistry by transferring an electron to a pheophytin acceptor (Pheo). The charge-separated state is rapidly stabilized by reduction of $P680^+$ and oxidation of $Pheo^-$, which prepares the reaction center for subsequent turnovers. The oxidant of Pheo is a bound quinone (Q_A) that shuttles electrons to an exchangeable quinone (Q_B). The direct electron donor to $P680^+$ is a redox-active tyrosine (Y_Z) that works in concert with a tetramanganese (Mn_4) cluster to abstract electrons from H_2O. The Mn_4 cluster and Y_Z, along with Ca^{2+} and Cl^- cofactors, are thought to be the active site of water oxidation and together are known as the oxygen-evolving complex (OEC) of PSII (reviewed in ref 1; see Figure 1). In accumulating the four oxidizing equivalents necessary to oxidize two H_2O molecules, the Mn_4 cluster cycles through five oxidation states which are referred to as S_n states (where $n =$ 0−4 and denotes the number of stored oxidizing equivalents). S_1 is the dark stable state, and O_2 is released spontaneously during the S_4 to S_0 state transition.

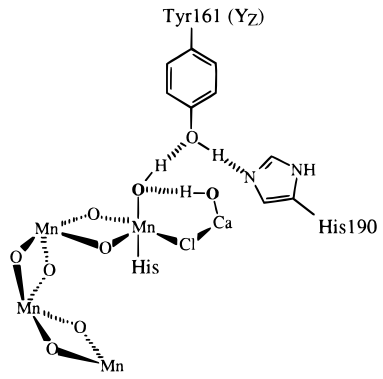

Figure 1. Structural model of the OEC including the proposed hydrogen-bonding network between the Mn_4 cluster, Y_Z, and the Ca^{2+}/Cl^- cofactors (adapted from ref 60).

The molecular structure of PSII has not yet been determined; thus, structural and functional characterization of the OEC has relied on a number of biophysical methods, most notably X-ray absorption and electron paramagnetic resonance (EPR) spectroscopy (reviewed in refs 2−6). The forms of the Mn_4 cluster

[†] University of California.
[‡] Yale University.
[§] Current address: Xanthon, Inc., P.O. Box 12296, Research Triangle Park, NC 27709.

(1) Debus, R. J. *Biochim. Biophys. Acta* **1992**, *1102*, 269−352.
(2) Brudvig, G. W. *Adv. Chem. Ser.* **1995**, *246*, 249−263.

10.1021/ja9932885 CCC: $19.00
Published on Web 02/09/2000

most commonly studied by spectroscopy are the S_1 and S_2 states because they can be generated quantitatively in highly concentrated (μM to mM) samples. X-ray spectroscopic studies of the OEC have revealed the following: (1) extended X-ray absorption fine structure (EXAFS) data for the S_1 state indicate Mn−Mn distances of 2.7 and 3.3 Å within the Mn_4 cluster and (2) X-ray absorption near edge structure (XANES) results for the S_1 state suggest a $Mn^{III}_2Mn^{IV}_2$ valence. Based on these results and the Mn−Mn exchange couplings required to explain the spin states of the various S states, the Mn_4 cluster has been proposed to be an asymmetric dimer of di-μ-oxo-bridged manganese dimers ($Mn^{III}-(\mu\text{-}O)_2-Mn^{III}$ and $Mn^{IV}-(\mu\text{-}O)_2-Mn^{IV}$) joined by a $Mn^{III}-(\mu\text{-}O)-Mn^{IV}$ bond[7−11] (reviewed in refs 3 and 6). EPR spectroscopy has also provided a wealth of structural information about the OEC (reviewed in refs 2, 4, and 12). Most EPR studies have focused on the S_2 state of the Mn_4 cluster. The S_2 state is an odd-electron state that displays two distinct types of EPR signals corresponding to two different spin states of the cluster: the $g \sim 2$ multiline ($S = {}^1/_2$) and the $g = 4.1$ ($S = {}^5/_2$) signals. In contrast, the S_1 state is an integer-spin state that cannot be detected directly by conventional EPR methods. EPR studies of the OEC have revealed the following: (1) H_2O is coordinated to the Mn_4 cluster in the S_2 state;[13] (2) ammonia can replace a bridging oxo in the Mn_4 cluster;[14] and (3) the Mn_4 cluster is coordinated by at least one histidine.[15,16]

Vibrational spectroscopy has also aided in the characterization of the OEC structure by identifying modes that reflect the coordination environment of the Mn_4 cluster. Fourier transform infrared (FTIR) measurements of the S_1-to-S_2 transition in ^{15}N-labeled PSII have enabled tentative assignments of COO^- stretches to glutamic acid or aspartic acid residues that ligate the Mn_4 cluster.[17−19] Based on D_2O/H_2O exchange studies, one of these carboxylate ligands has been further assigned as being hydrogen bonded to a H_2O molecule that is coordinated to the Mn_4 cluster.[20] Other bands identified in the S_2-minus-S_1 difference spectrum have been proposed to be amide I (CO stretch) and amide II (NH bend/CN stretch) stretches of the protein backbone that are influenced by the oxidation state of the Mn_4 cluster.[18] FTIR measurements on Y_Z have provided direct evidence of structural coupling between Y_Z and the Mn_4 cluster.[21] Unfortunately, the low-frequency IR region (<1000 cm^{-1}), which is of greatest interest for detecting Mn−ligand vibrations, has remained largely inaccessible for biological samples because of water absorption and other technical limitations. Recently, however, Chu et al. succeeded in measuring several low-frequency vibrational modes associated with the S_1 and S_2 states of the OEC by performing FTIR measurements on partially dehydrated PSII samples using a system optimized for low-frequency measurements.[22] While these measurements represent a significant advance, the frequency range did not extend below 550 cm^{-1} where a number of Mn-based vibrational modes are expected to appear.[23−25]

Like FTIR, resonance Raman (RR) spectroscopy has been used to identify vibrational modes within PSII. RR has the advantage that it can probe selectively chromophores within the protein complex depending on the excitation energy utilized. The technique of shifted-excitation Raman difference spectroscopy (SERDS)[26,27] is particularly useful because it mitigates fluorescence interference, thus permitting acquisition of RR spectra for highly fluorescent proteins such as the bacterial photosynthetic reaction center[28−31] and PSII.[32] Until recently, SERDS had seen limited use in characterizing PSII cofactors because the strong absorptions of the numerous (∼40) light-harvesting chlorophyll (Chl) molecules present in the core complex overlap the absorptions of other cofactors. However, for cofactors absorbing in the near-IR (NIR) region, NIR-excitation SERDS provides a way to circumvent this limitation. For example, NIR-excitation SERDS has been used to examine the Chl_Z cation in PSII and to identify its axial ligand.[32] NIR-excitation SERDS has also been used to measure selectively preresonance Raman (PRR) scattering from the core Chls in photosystem I (PSI).[33] Thus far, however, RR techniques have not been used to probe the OEC of PSII. To our knowledge, the only Raman experiments previously reported for the OEC are early surface-enhanced Raman scattering (SERS) studies by Cotton and co-workers.[34] The SERS spectra, which were

(3) Yachandra, V. K.; Sauer, K.; Klein, M. P. *Chem. Rev.* **1996**, *96*, 2927−2950.
(4) Britt, R. D. In *Oxygenic Photosynthesis: The Light Reactions*; Ort, D. R., Yocum, C. F., Eds.; Kluwer Academic Publishers: Dordrecht, The Netherlands, 1996; pp 137−164.
(5) Diner, B. A.; Babcock, G. T. In *Oxygenic Photosynthesis: The Light Reactions*; Ort, D. R., Yocum, C. F., Eds.; Kluwer Academic Publishers: Dordrecht, The Netherlands, 1996; pp 213−247.
(6) Penner-Hahn, J. E. *Structure Bonding* **1998**, *90*, 1−36.
(7) George, G. N.; Prince, R. C.; Cramer, S. P. *Science* **1989**, *243*, 789−791.
(8) Kusunoki, M.; Ono, T.; Matsushita, T.; Oyanagi, H.; Inoue, Y. *J. Biochem.* **1990**, *108*, 560−567.
(9) Penner-Hahn, J. E.; Fronko, R. M.; Pecoraro, V. L.; Yocum, C. F.; Betts, S. D.; Bowlby, N. R. *J. Am. Chem. Soc.* **1990**, *112*, 2549−2557.
(10) MacLachlan, D. J.; Hallahan, B. J.; Ruffle, S. V.; Nugent, J. H. A.; Evans, M. C. W.; Strange, R. W.; Hasnain, S. S. *J. Biochem.* **1992**, *285*, 569−576.
(11) Yachandra, V. K.; DeRose, V. J.; Latimer, M. J.; Mukerji, I.; Sauer, K.; Klein, M. P. *Science* **1993**, *260*, 675−678.
(12) Miller, A.-F.; Brudvig, G. W. *Biochim. Biophys. Acta* **1991**, *1056*, 1−18.
(13) Fiege, R.; Zweygart, W.; Bittl, R.; Adir, N.; Renger, G.; Lubitz, W. *Photosynth. Res.* **1996**, *48*, 227−237.
(14) Britt, R. D.; Zimmermann, J.-L.; Sauer, K.; Klein, M. P. *J. Am. Chem. Soc.* **1989**, *111*, 3522−3532.
(15) DeRose, V. J.; Yachandra, V. K.; MeDermott, A. E.; Britt, R. D.; Sauer, K.; Klein, M. P. *Biochemistry* **1991**, *30*, 1335−1341.
(16) Tang, X.-S.; Diner, B. A.; Larsen, B. S.; Gilchrist, M. L.; Lorigan, G. A.; Britt, R. D. *Proc. Natl. Acad. Sci. U.S.A.* **1994**, *91*, 704−708.
(17) Noguchi, T.; Ono, T.; Inoue, Y. *Biochemistry* **1992**, *31*, 5953−5956.
(18) Noguchi, T.; Ono, T.; Inoue, Y. *Biochim. Biophys. Acta* **1995**, *1228*, 189−200.
(19) Steenhuis, J. J.; Barry, B. A. *J. Phys. Chem. B* **1997**, *101*, 6652−6660.
(20) Noguchi, T.; Ono, T.; Inoue, Y. *Biochim. Biophys. Acta* **1995**, *1232*, 59−66.
(21) Noguchi, T.; Inoue, Y.; Tang, X.-S. *Biochemistry* **1997**, *36*, 14705−14711.
(22) Chu, H.-A.; Gardner, M. T.; O'Brien, J. P.; Babcock, G. T. *Biochemistry* **1999**, *38*, 4533−4541.
(23) Ross, S. D. In *Inorganic Infrared and Raman Spectra*; McGraw-Hill: London, 1972.
(24) Davidson, G. *Spectroscopic Properties of Inorganic and Organometallic Compounds*; The Royal Society of Chemistry, U.K.: London, 1997; Vol. 30.
(25) Nakamoto, K. In *Infrared and Raman Spectra of Inorganic and Coordination Compounds*, 5th ed.; John Wiley & Sons: New York, 1997.
(26) Shreve, A.; Cherepy, N. J.; Franzen, S.; Boxer, S. G.; Mathies, R. A. *Proc. Natl. Acad. Sci. U.S.A.* **1991**, *88*, 11207−11211.
(27) Shreve, A.; Cherepy, N. J.; Mathies, R. A. *Appl. Spectrosc.* **1992**, *46*, 707−711.
(28) Cherepy, N. J.; Shreve, A. P.; Moore, L. J.; Franzen, S.; Boxer, S. G.; Mathies, R. A. *J. Phys. Chem.* **1994**, *98*, 6023−6029.
(29) Palaniappan, V.; Schenck, C. C.; Bocian, D. F. *J. Phys. Chem.* **1995**, *99*, 17049−17058.
(30) Cherepy, N. J.; Shreve, A. P.; Moore, L. J.; Boxer, S. G.; Mathies, R. A. *J. Phys. Chem. B* **1997**, *101*, 3250−3260.
(31) Czarnecki, K.; Diers, J. R.; Chynwat, V.; Erikson, J. P.; Frank, H. A.; Bocian, D. F. *J. Am. Chem. Soc.* **1997**, *119*, 415−426.
(32) (a) Cua, A.; Stewart, D. H.; Brudvig, G. W.; Bocian, D. F. *J. Am. Chem. Soc.* **1998**, *120*, 4532−4533. (b) Stewart, D. H.; Cua, A.; Chisholm, D. A.; Diner, B. A.; Bocian, D. F.; Brudvig, G. W. *Biochemistry* **1998**, *37*, 10040−10046.
(33) Stewart, D. H.; Cua, A.; Bocian, D. F.; Brudvig, G. W. *J. Phys. Chem. B* **1999**, *103*, 3758−3764.

obtained using visible excitation, exhibited a single low-frequency band that could not be definitively attributed to the Mn_4 cluster.

Recently, several papers have appeared that describe a conversion between the multiline and $g = 4.1$ forms of the S_2 state of the Mn_4 cluster induced by NIR illumination. This conversion has an action spectrum with $\lambda_{max} \sim 820$ nm and has been assigned as an electronic transition of the Mn_4 cluster corresponding to a spin-state change or an intervalence electron-transfer event.[35] The photoinduced conversion from the multiline to $g = 4.1$ form occurs optimally at ~150 K. Illumination at lower temperatures (<65 K) does not effect conversion to the $g = 4.1$ form, but instead provides evidence for a third form of the S_2 state (with $S = {}^5/_2$) that is an intermediate between the multiline and $g = 4.1$ forms.[36] The requirement for NIR light to activate the conversion from the multiline to $g = 4.1$ form is evidence that the latter form is an electronically modified version of the S_2 state favored by certain structural arrangements of the OEC rather than a precursor to the multiline form.[35,36] Although controversial, the presence of a NIR transition of the Mn_4 cluster has been suggested previously based on the observation of a broad, weak absorption band ($\lambda_{max} \sim 780$ nm) in the S_2-minus-S_1 difference spectrum.[37,38] Similar NIR bands have been reported for di-μ-oxo-bridged Mn_2 inorganic model complexes.[39,40] The NIR band of the di-μ-oxo $Mn^{III}Mn^{IV}$ structural unit has been attributed to a superposition of a number of Mn d−d and oxo-to-Mn charge-transfer bands.[41]

The fact that the OEC in PSII exhibits a NIR absorption band affords the possibility of probing selectively the vibrational structure of the complex using RR spectroscopy. Toward this end, we initiated a NIR-excitation SERDS study of the S_1 and S_2 states of the OEC. These studies used a broad-based approach that included (1) consecutive illumination/dark-adaptation treatments to cycle between the S_1 and S_2 states, (2) a survey of the NIR-excitation-wavelength dependence of the Raman scattering, (3) measurement of the effect of D_2O/H_2O exchange, and (4) examination of the effects of NIR irradiation at reduced temperatures. The NIR-excitation RR studies reveal several unique vibrational features that are attributed to Mn−ligand modes. These data provide important constraints that aid in refining structural models of the OEC of PSII.

Materials and Methods

Sample Preparation. Cells of *Synechocystis* PCC 6803 were grown photoheterotrophically at 30 °C in 18 L carboys containing BG-11 medium[42] supplemented with 5 mM glucose and bubbled with 5% CO_2 in air. O_2-evolving PSII core complexes were isolated from these cells using the procedure of Tang and Diner.[43] Both O_2-evolution assays and SDS-polyacrylamide gel electrophoresis indicated low levels (<10%) of PSI contamination. Mn-depleted PSII complexes were prepared by treatment with 5 mM NH_2OH and 5 mM EDTA in Chenaie's buffer A (50 mM MES, pH 6.5, 15 mM NaCl, 1 mM $CaCl_2$, 0.4 M sucrose) plus 0.03% *n*-dodecyl-β-D-maltoside (DM) followed by washing with 5 mM EDTA in buffer A to remove unbound Mn-(II).[44] The PSII core complexes were stored in 50 mM MES, pH 6.0, 20 mM $CaCl_2$, 10 mM NaCl, 20% (v/v) glycerol, and 0.03% DM at 77 K in the dark until further use. Determinations of Chl concentration were made by extraction into methanol and using $\epsilon_{665} = 79.24$ mL/(mg Chl-cm) for Chl *a* in methanol.[45]

Raman Spectroscopy. The Raman measurements were made at reduced temperature (200 K and lower) on highly concentrated, glassy samples contained in 1 mm i.d. capillary tubes. The PSII samples were at a concentration of 10−20 mg of Chl/mL in 50 mM MES, pH 6.0, 20 mM $CaCl_2$, 10 mM NaCl, 20% (v/v) glycerol containing 1 mM $K_3Fe(CN)_6$. The D_2O-exchanged samples were prepared in the same buffers using D_2O instead of H_2O. Raman spectra for both the O_2-evolving and Mn-depleted PSII samples were collected for dark-adapted and illuminated samples. The dark-adapted samples were prepared by placing them in the dark at 0 °C for several hours. In untreated, dark-adapted O_2-evolving PSII, the OEC is primarily in the S_1 resting state.[46,47] The illuminated samples were prepared by reducing the temperature to 200 K and subjecting them to 15 m of continuous white light irradiation from a focused 200 W quartz/halogen lamp. Continuous illumination at 200 K photooxidizes the OEC to the S_2 state in high yield.[48]

The Raman sampling accessories, spectrometer, and laser systems used for the present studies have been described previously.[49,50] The majority of the Raman spectra were collected with $\lambda_{ex} = 820$ nm. A number of different studies were performed using this excitation wavelength. (1) Data sets were obtained with 30 min, 1 h, 2 h, and 5 h of signal averaging (15, 30, 60, or 150 × 2 m scans). (2) Data sets were obtained using different laser powers in the 2−5 mW range. At all of these powers, the laser beam was loosely focused (beam diameter ~100 μm) (3) Data sets were acquired several (3−5) times for a particular sample. In all cases, the general features observed in the spectra were found to be identical. The fact that the sample was robust under the longest data acquisition times (5 h) and highest powers (~5 mW; power density ~65 W/cm^2) investigated led us to obtain the spectra reported herein under these conditions (to optimize S/N), unless otherwise noted. For the studies at other excitation wavelengths and studies of light/dark adaptation (vide infra), each Raman data set was obtained with 2 h of signal averaging. Cosmic spikes in the individual scans were removed prior to coaddition of the scans. The spectral resolution was ~2 cm^{-1}. All spectra are unpolarized. The spectral data were calibrated using the known frequencies of fenchone.

All of the Raman spectra were acquired using the SERDS technique to reduce the level of interference from fluorescence.[26,27] The application of the SERDS method to photosynthetic proteins has been described previously in detail.[26−31] Briefly, each data set is acquired at two excitation wavelengths that differ by a small wavenumber increment (typically 10 cm^{-1}). [The 5 h (or 2 h) data acquisition time indicated above is for each of the two data sets required to yield a background-free Raman difference (SERDS) spectrum.] The Raman spectra presented herein were obtained by subtracting the initial spectrum from the shifted spectrum. The spectral window is defined by the initial spectrum and corresponds to the wavenumber axis in the figures. The normal Raman spectrum is then reconstructed from the SERDS data

(34) (a) Seibert, M.; Cotton, T. M. *FEBS Lett.* **1985**, *182*, 34−38. (b) Seibert, M.; Cotton, T. M.; Metz, J. G. *Biochim. Biophys. Acta* **1988**, *934*, 235−246.
(35) (a) Boussac, A.; Girerd, J.-J.; Rutherford, A. W. *Biochemistry* **1996**, *35*, 6984−6989. (b) Baxter, R.; Krausz, E.; Wydrzynski, T.; Pace, R. J. *J. Am. Chem. Soc.* **1999**, *121*, 9451−9452.
(36) Boussac, A.; Un, S.; Horner, O.; Rutherford, A. W. *Biochemistry* **1998**, *37*, 4001−4007.
(37) Dismukes, G. C.; Mathis, P. *FEBS Lett.* **1984**, *178*, 51−54
(38) Velthuys, B. R. *Biochim. Biophys. Acta* **1988**, *933*, 249−257.
(39) Cooper, S. R.; Calvin, M. *J. Am. Chem. Soc.* **1977**, *99*, 6623−6630.
(40) Sheats, J. E.; Czernuszewicz, R. S.; Dismukes, G. C.; Rheingold, A. L.; Petrouleas, V.; Stubbe, J.; Armstrong, W. H.; Beer, R. H.; Lippard, S. J. *J. Am. Chem. Soc.* **1987**, *109*, 1435−1444.
(41) Gamelin, D. R.; Kirk, M. L.; Stemmler, T. L.; Pal, S.; Armstrong, W. H.; Penner-Hahn, J. E.; Solomon, E. I. *J. Am. Chem. Soc.* **1994**, *116*, 2392−2399.
(42) Rippka, R.; Deruelles, J.; Waterbury, J. B.; Herdman, M.; Stanier, R. Y. *J. Gen. Microbiol.* **1979**, *111*, 1−61.
(43) Tang, X.-S.; Diner, B. A. *Biochemistry* **1994**, *33*, 4594−4603.
(44) Tamura, N.; Cheniae, G. *Biochim. Biophys. Acta* **1987**, *890*, 179−194.
(45) Lichtenthaler, H. K. *Methods Enzymol.* **1987**, *148*, 350−382.
(46) Beck, W. F.; de Paula, J. C.; Brudvig, G. W. *Biochemistry* **1985**, *24*, 3035−3043.
(47) Koulougliotis, D.; Hirsh, D. J.; Brudvig, G. W. *J. Am. Chem. Soc.* **1992**, *114*, 8322−8323.
(48) Brudvig, G. W.; Casey, J. L.; Sauer, K. *Biochim. Biophys. Acta* **1983**, *723*, 366−371.
(49) Palaniappan, V.; Aldema, M. A.; Frank, H. A.; Bocian, D. F. *Biochemistry* **1992**, *31*, 11050−11058.
(50) Palaniappan, V.; Martin, P. C.; Chynwat, V.; Frank, H. A.; Bocian, D. F. *J. Am. Chem. Soc.* **1993**, *115*, 12035−12049.

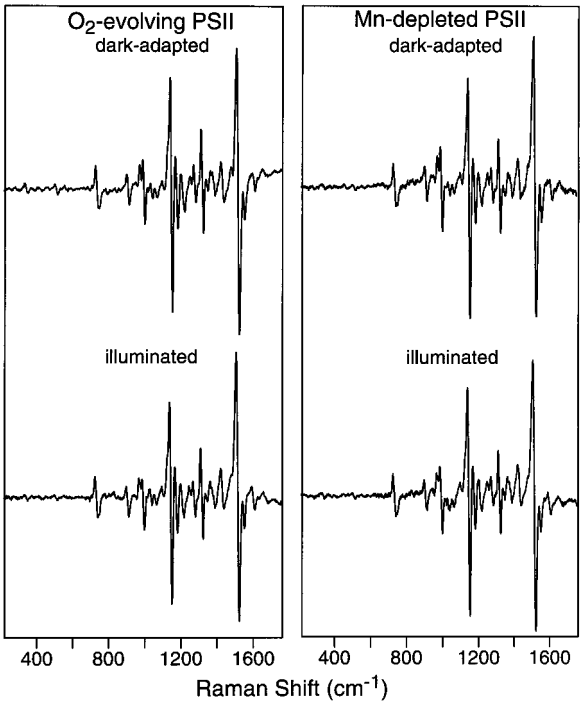

Figure 2. NIR-excitation (λ_{ex} = 820 nm) SERDS data (220−1760 cm^{-1}) obtained for dark-adapted and illuminated O_2-evolving (left panel) and Mn-depleted (right panel) PSII at 200 K.

by fitting the latter to a series of derivative-shaped functions (in this case, difference bands generated from Gaussian functions) of arbitrary frequency, amplitude, and width. The frequencies marked in the figures correspond to the positions of the bands used in the fits and, thus, do not necessarily correspond to the peak maxima for overlapping bands. In addition, certain bands are marked that are not clearly resolved in the spectra. These bands are indicated because their inclusion noticeably improved the quality of the fits to the SERDS data based on the residuals (observed spectra minus fits).

Results

The NIR-excitation Raman scattering characteristics of O_2-evolving PSII were investigated under a variety of conditions (dark-adapted versus illuminated, different excitation wavelengths, and D_2O versus H_2O solutions). As a control, Raman spectra were also acquired for Mn-depleted PSII under selected conditions. The initial Raman studies surveyed the scattering characteristics in the 220−1760 cm^{-1} region and used several different excitation wavelengths in the 790−830 nm range. Based on the results of the initial studies, the investigation was ultimately focused on the low-frequency (below 600 cm^{-1}) region and primarily used excitation at 820 nm. We first describe the general features of the NIR-excitation Raman spectra of PSII. We then turn to specific studies of the low-frequency spectral region. The characteristics of the raw (unsmoothed) SERDS data are exclusively used in the description of these results. Finally, we present the normal Raman spectra that are reconstructed from the SERDS data sets.

General Features of the NIR-Excitation Raman Spectra. The NIR-excitation (λ_{ex} = 820 nm) raw (unsmoothed) SERDS data (220−1760 cm^{-1}) for dark-adapted and illuminated O_2-evolving PSII are shown in Figure 2, left panel; the analogous data obtained for Mn-depleted PSII are shown in Figure 2, right panel. The data shown were obtained in four ∼450 cm^{-1} wide overlapping spectral windows. The spectra observed at other excitation wavelengths are generally similar (not shown). The spectra shown in Figure 2 were obtained at 200 K. Spectra were also obtained at lower temperatures (150 and 30 K); however, these spectra are similar to those shown in Figure 2.

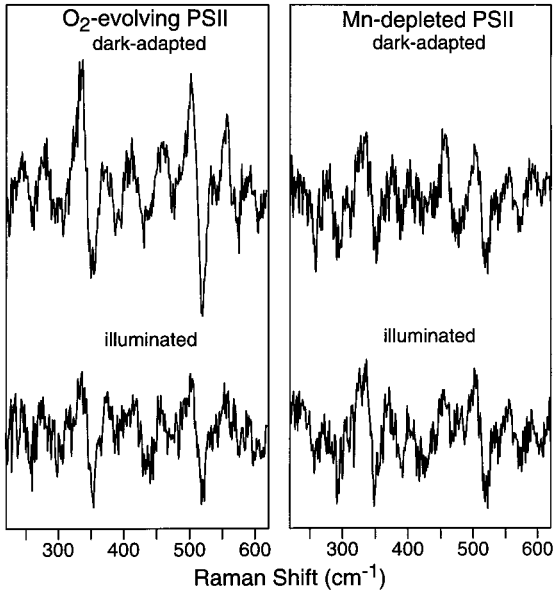

Figure 3. Expansion of the low-frequency (220−620 cm^{-1}) NIR-excitation (λ_{ex} = 820 nm) SERDS data obtained for dark-adapted and illuminated O_2-evolving (left panel) and Mn-depleted (right panel) PSII at 200 K.

Inspection of the SERDS data in Figure 2 reveals that the Raman scattering characteristics of dark-adapted and illuminated O_2-evolving PSII are generally similar to one another and similar to those of dark-adapted and illuminated Mn-depleted PSII. In the 600−1760 cm^{-1} region, the Raman features exhibited by all four samples are so similar as to be deemed identical within experimental error. In this regard, previous NIR-excitation Raman studies of Mn-depleted PSII have shown that all of the spectral features observed are consistent with those expected for Chl *a*.[32] Strong Raman scattering is observed from Chl *a* with excitation in the 800 nm region despite the fact that these excitation wavelengths are relatively far from the absorption maximum for these pigments in the PSII core complex (which is near 673 nm). The preresonance Raman (PRR) scattering from Chl *a* is large because the sample concentration is high and there are a large number (∼40) of Chl *a* molecules in the PSII core complex. The similarity between the SERDS data for the O_2-evolving (both dark adapted and illuminated) and Mn-depleted samples in the 600−1760 cm^{-1} region strongly suggests that all of the Raman features observed for the former samples are also due to PPR from Chl *a*. This result does not preclude the presence of features from other scattering centers in this spectral region. However, if these features are present, they are completely obscured by the strong PRR scattering from Chl *a*.

Closer inspection of the low-frequency (below 600 cm^{-1}) SERDS data for dark-adapted versus illuminated O_2-evolving PSII reveals certain clear differences in the spectra. To facilitate comparison, the SERDS data obtained for O_2-evolving PSII in the 220−620 cm^{-1} range are shown on an expanded scale in Figure 3, left panel; the analogous data for Mn-depleted PSII are also included in Figure 3, right panel. The SERDS data for dark-adapted O_2-evolving PSII are distinguished from those of the illuminated sample by enhanced intensity in certain features (e.g., near 350 and 520 cm^{-1}) and the presence of additional features (e.g., near 300 cm^{-1}). In contrast, the SERDS traces for dark-adapted and illuminated Mn-depleted PSII are essentially identical with one another. In addition, the SERDS

trace for illuminated O_2-evolving PSII is generally quite similar to those of Mn-depleted PSII. Collectively, these observations indicate that the NIR-excitation Raman spectrum of dark-adapted O_2-evolving PSII contains features from scattering centers in addition to those that contribute to the spectrum of the Mn-depleted complex (Chl *a* is the only likely source of Raman scattering for the latter complex (vide infra)).

The S_1 state of the Mn_4 cluster is the likely candidate for the new scattering center in dark-adapted O_2-evolving PSII for several reasons. First, the S_1 state is the dark-stable state of the Mn_4 cluster; both higher and lower S states decay to S_1 in the dark in tens of minutes or less (reviewed in ref 2). Second, PSII depleted of Mn by NH_2OH treatment retains all of the other electron-transfer species in the reaction center;[51] therefore, the only difference between O_2-evolving and Mn-depleted PSII is the presence of the Mn_4 cluster and its associated Ca^{2+} and Cl^- cofactors in the O_2-evolving sample. Third, the only components of dark-adapted O_2-evolving PSII that change oxidation state upon 200 K illumination are Q_A and the Mn_4 cluster. Q_A^- is not expected to display vibrational bands below 700 cm^{-1},[22] and its contribution is ruled out by the lack of change upon illumination of Mn-depleted PSII (which also forms Q_A^- upon illumination at 200 K). Furthermore, it should be noted that our previous NIR-excitation Raman studies of Mn-depleted PSII have shown that the laser exciting beam does not induce any actinic effects under the conditions of the experiments.[32a] The excitation energies are apparently too low to produce any appreciable charge separation. Collectively, these considerations suggest that the S_1 state of the Mn_4 cluster is the scatterer giving rise to the additional low-frequency bands in dark-adapted O_2-evolving PSII. The fact that illumination of the O_2-evolving sample and conversion to the S_2 state of the Mn_4 cluster bleaches the additional SERDS features likewise indicates that there is minimal (or negligible) contribution to the NIR Raman spectrum from the S_2 state of the Mn_4 cluster.

Specific Features of the Low-Frequency NIR-Excitation Raman Spectra. To investigate further the low-frequency (220−620 cm^{-1}) NIR-excitation Raman scattering characteristics of O_2-evolving PSII, a number of other experiments were performed. These studies investigated the effects of (1) light and dark cycling, (2) excitation wavelength changes, (3) D_2O/H_2O exchange, and (4) NIR irradiation at reduced temperatures (150 and 30 K). The results of these experiments are described in more detail below.

1. Light/Dark Cycling. O_2-evolving PSII was subjected to a series of illumination and dark-adaptation treatments to cycle between the S_1 and S_2 states of the OEC. In the first series of experiments, the illuminated O_2-evolving PSII sample was warmed to 0 °C, re-dark adapted for several hours, and recooled to 200 K, and the low-frequency Raman data were reacquired. The SERDS data obtained for the re-dark-adapted sample are compared with those of the initially dark-adapted and illuminated samples in Figure 4. As can be seen, the SERDS data for the re-dark-adapted sample (bottom trace) are quite similar to those of the original dark-adapted sample (top trace). The S/N ratio for the re-dark-adapted sample is somewhat lower than that for the original dark-adapted sample because the data for the former sample were acquired with 2 h of signal averaging whereas those for the latter were acquired with 5 h of averaging. In the second series of experiments, the sample was subjected to repeated illumination/dark-adaptation cycles. The Raman spectra were reacquired for re-dark-adapted and illuminated samples in each cycle. The SERDS data obtained on successive cycles were generally similar to those shown in Figure 4 (top and middle traces). However, after several cycles (3−5), re-dark adaptation failed to restore the spectrum characteristic of the original dark (and first re-dark)-adapted PSII sample. From this point on, the SERDS traces generally resembled that of illuminated PSII (Figure 4, middle trace). The damping of the differential S_1/S_2 state spectra upon repeated illumination and dark adaptation is consistent with O_2-evolution measurements on *Synechocystis* PSII core complexes that indicate that the process of repeated freezing/thawing/dark adaptation causes some loss of function of the OEC, independent of whether the sample is subjected to NIR laser irradiation.[52]

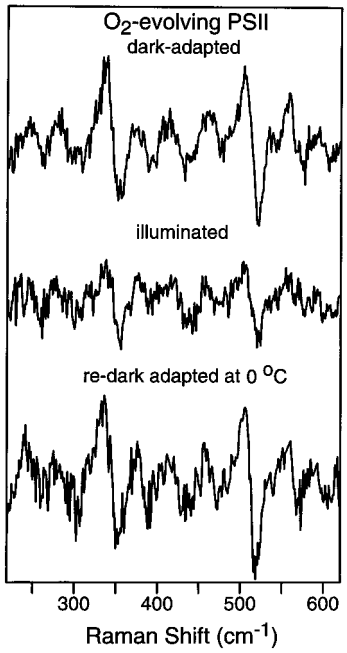

Figure 4. Low-frequency (220−620 cm^{-1}) NIR-excitation (λ_{ex} = 820 nm) SERDS data for re-dark-adapted (bottom trace) versus dark-adapted (top trace) and illuminated (middle trace) O_2-evolving PSII at 200 K.

2. Excitation Wavelength Changes. The NIR-excitation wavelength dependence of the low-frequency Raman scattering from dark-adapted O_2-evolving PSII was examined in detail in the 800−825 nm range. The low-frequency SERDS data sets obtained with λ_{ex} = 824, 820, and 816 nm are compared in Figure 5. The spectra shown in this figure have a lower S/N than those shown in Figures 2−4 because the data acquisition time was shorter (2 versus 5 h for a single SERDS data set). The SERDS data sets obtained at shorter excitation wavelengths (near 800 nm) are not shown because the quality of these data was generally poor due to the fact that the intensity of the background fluorescence from Chl *a* in the PSII core complex steeply increases toward shorter wavelength. Although the range of excitation wavelengths over which viable SERDS data can be acquired is rather limited, certain trends are observable in the spectra: (1) with λ_{ex} = 824 nm, the Raman signals are generally weaker than those observed with λ_{ex} = 820 and 816 nm, and (2) the differences between the data obtained with λ_{ex} = 820 versus 816 nm are less apparent. However, the relative intensities of certain Raman features appear to be different in these two data sets. For example, the ∼300 cm^{-1} SERDS feature that distinguishes dark-adapted from illuminated O_2-evolving PSII is much more pronounced with λ_{ex} = 820 nm than with

(51) Buser, C. A.; Thompson, L. K.; Diner, B. A.; Brudvig, G. W. *Biochemistry* **1990**, *29*, 8977−8985.

(52) (a) Stewart, D. H., Ph.D. Thesis, Yale University, New Haven, CT, 1998. (b) Reifler, M. J.; Brudvig, G. W. Unpublished results.

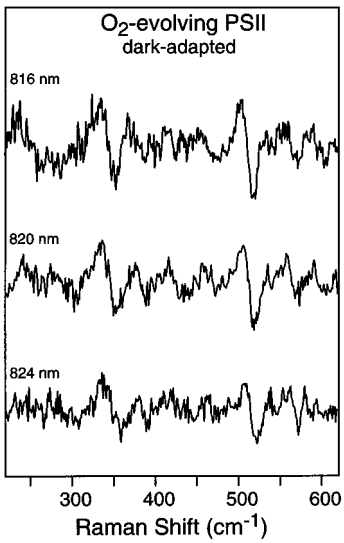

Figure 5. Excitation-wavelength dependence of the low-frequency (220−620 cm^{-1}) NIR-excitation SERDS spectra of dark-adapted O_2-evolving PSII at 200 K.

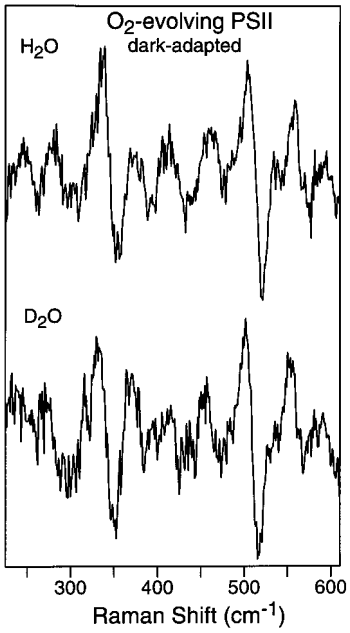

Figure 6. Low-frequency (220−620 cm^{-1}) NIR-excitation ($\lambda_{ex} = 820$ nm) SERDS data for dark-adapted O_2-evolving PSII in H_2O (top trace) versus D_2O (bottom trace) at 200 K.

$\lambda_{ex} = 816$ nm. These observations qualitatively suggest that the Raman intensities of features associated with the S_1 state of the Mn_4 cluster maximize with $\lambda_{ex} \sim 820$ nm.

3. D_2O/H_2O Exchange. The low-frequency NIR-excitation Raman scattering characteristics of dark-adapted O_2-evolving PSII were examined in D_2O versus H_2O. The SERDS traces for these samples are compared in Figure 6. The overall features of the spectra are similar in the two solvents. However, closer examination reveals that certain spectral features are shifted in D_2O. For example, the ∼300 cm^{-1} feature that is characteristic of dark-adapted PSII is clearly downshifted in D_2O. Other spectral differences are apparent in the 400−450 cm^{-1} spectral region of the D_2O versus H_2O SERDS data.

4. NIR Irradiation at Reduced Temperatures. Spectral data for a white-light-illuminated O_2-evolving sample, in which the Mn_4 cluster is in the S_2 state, were acquired both before and after the sample was irradiated with NIR light (∼820 nm) at 150 and 30 K. These experiments were performed to determine whether the conversion of the S_2 state from the form yielding the multiline EPR signal to that yielding the $g = 4.1$ signal could be detected in the Raman spectrum. In all cases, the SERDS data sets obtained before and after NIR irradiation were identical with those shown for the illuminated sample in Figure 3.

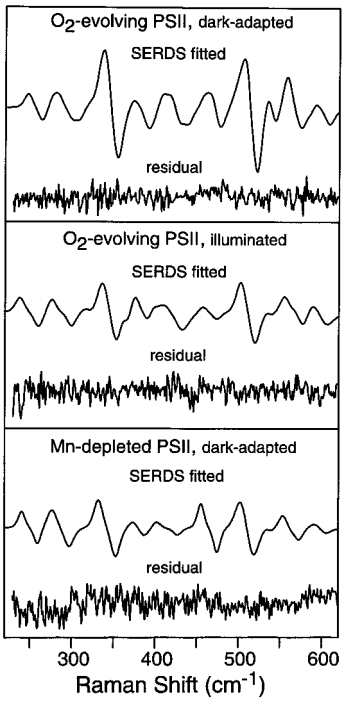

Figure 7. Fits of the low-frequency (220−620 cm^{-1}) NIR-excitation ($\lambda_{ex} = 820$ nm) SERDS data for dark-adapted O_2-evolving PSII (top panel), illuminated O_2-evolving PSII (middle panel), and dark-adapted Mn-depleted PSII (bottom panel). The residuals obtained by subtracting the fits from the raw SERDS data shown in Figure 3 are also shown beneath each fitted SERDS trace.

Reconstructed Spectra. Figure 7 shows the fits of the raw SERDS data sets for dark-adapted and illuminated O_2-evolving PSII and dark-adapted Mn-depleted PSII shown in Figure 3. The fits for the illuminated Mn-depleted sample are not shown because the SERDS traces are essentially identical with those of the dark-adapted sample. Figure 8 shows the fits for the raw SERDS data sets for dark-adapted O_2-evolving PSII in H_2O and D_2O shown in Figures 6. The SERDS residuals (observed minus fitted data) are also included for each of the data sets in Figures 7 and 8. The relatively small residuals compared with the SERDS intensities are indicative of the excellent fidelity of the fits for all of the PSII samples. Figures 9 and 10 depict the low-frequency Raman spectra reconstructed from the SERDS data sets in Figures 7 and 8, respectively. The Raman bands observed for the PSII core complex are summarized in Table 1.

Examination of Figure 9 and Table 1 reveals the following features of the Raman spectra. The spectrum of dark-adapted O_2-evolving PSII exhibits bands at 263, 299, 309, 327, 348, 354, 367, 377, 391, 428, 438, 475, 476, 511, 522, 543, 564, 575, 587, and 608 cm^{-1}. The bands at 309, 348, 377, 438, 476, 511, and 587 cm^{-1} are unique to the spectrum of the dark-adapted complex. The most intense features at 348 and 511 cm^{-1} give rise to the enhanced intensities that are visible in the raw SERDS data in these spectral regions. Likewise, the unique feature at 309 cm^{-1} is associated with the new feature observed in the raw SERDS data in this region. The other bands at 377,

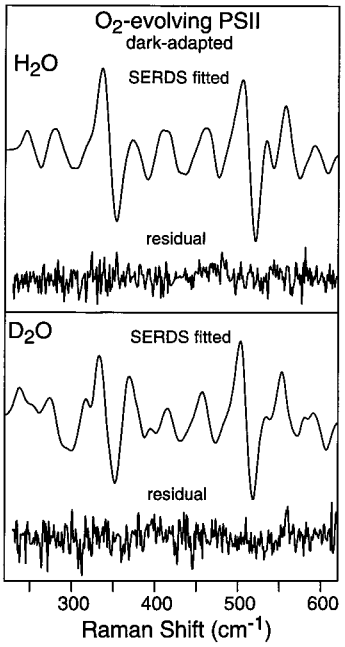

Figure 8. Fits of the low-frequency (220−620 cm^{-1}) NIR-excitation (λ_{ex} = 820 nm) SERDS data for dark-adapted O_2-evolving PSII in H_2O (top trace) versus D_2O (bottom trace). The residuals obtained by subtracting the fits from the raw SERDS data shown in Figure 6 are also shown beneath each fitted SERDS trace.

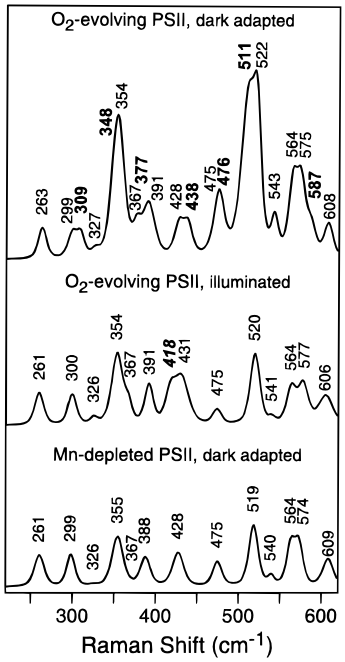

Figure 9. Comparison of the low-frequency (220−620 cm^{-1}) NIR-excitation (λ_{ex} = 820 nm) Raman spectra reconstructed from the fits of the SERDS data (Figure 7) for dark-adapted O_2-evolving PSII (top trace), illuminated O_2-evolving PSII (middle trace), and dark-adapted Mn-depleted PSII (bottom trace). The bands marked in bold in the top trace are unique to dark-adapted O_2-evolving PSII. The single band marked in bold in the middle trace is unique to illuminated O_2-evolving PSII.

438, 476, and 587 cm^{-1} were not clearly identified in the raw SERDS data sets; however, exclusion of these bands from the spectral reconstructions significantly reduces the quality of the fits. It should also be noted that it is not possible to obtain good fits to the SERDS data by eliminating any of the seven new

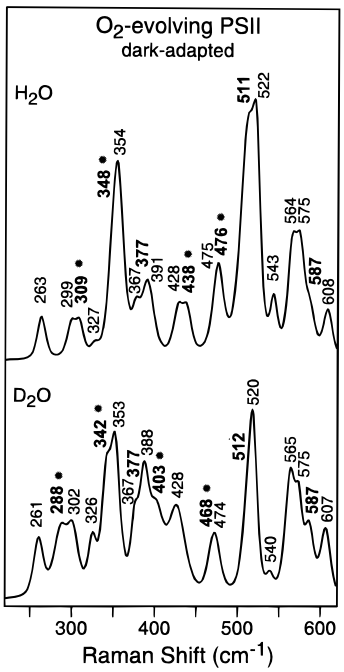

Figure 10. Comparison of the low-frequency (220−620 cm^{-1}) NIR-excitation (λ_{ex} = 820 nm) Raman spectra reconstructed from the fits of the SERDS data (Figure 8) for dark-adapted O_2-evolving PSII in H_2O (top trace) versus D_2O (bottom trace). The bands marked in bold are unique to the spectrum of dark-adapted O_2-evolving PSII. The bold bands marked by asterisks are sensitive to D_2O/H_2O exchange.

Table 1. Low-Frequency (<620 cm^{-1}) Raman Bands of PSII Observed with NIR Excitation[a,b]

O_2-evolving PSII		Mn-depleted PSII	
dark-adapted[b]	illuminated	dark-adapted	PSI[d]
263	261	261	261
299	300	299	301
309			
327	326	326	330
348			
354	354	355	355
367	367	367	
377			
391	391	388	391
	418[c]		413
428	431	428	430
438			
475	475	475	478
476			
511			
522	520	519	521
543	541	540	543
564	564	564	564
575	577	574	576
587			
608	606	609	608

[a] Obtained with λ_{ex} = 820 nm. [b] Bands listed in bold bleach upon illumination. [c] This band is unique to the spectrum of illuminated O_2-evolving PSII (see text). [d] Taken from ref 33.

bands and compensating for their elimination by altering the line widths of nearby and/or overlapping bands. Good fits can only be obtained in this fashion if highly asymmetric (rather than a simple Gaussian) bands are used in the simulations. Such band shapes are physically unrealistic. The other bands observed in the Raman spectrum of dark-adapted O_2-evolving PSII (263, 299, 327, 354, 367, 391, 428, 475, 522, 543, 564, 575, and 608 cm^{-1}) all have analogues in the spectra of both illuminated O_2-evolving PSII (261, 300, 326, 354, 367, 391, 431, 475, 520,

Table 2. Low-Frequency (<620 cm^{-1}) Raman Bands of Dark-Adapted O_2-Evolving PSII in D_2O versus H_2O[a,b]

H_2O	D_2O	H_2O	D_2O
309*	288*	476*	468*
348*	342*	511	512
377	377	587	587
438*	403*		

[a] Only those bands that bleach upon illumination are listed (see text). [b] Bands marked with an asterisk are sensitive to D_2O/H_2O exchange.

541, 564, 577, and 606 cm^{-1}) and Mn-depleted PSII (261, 299, 326, 355, 367, 388, 428, 475, 519, 540, 564, 574, and 609 cm^{-1}). In addition, these same bands are observed in the NIR-excitation Raman spectrum of dark-adapted PSI whose PRR scattering characteristics in the 200−1700 cm^{-1} frequency range were recently reported by our groups.[33] [The bands observed for PSI are also listed in Table 1.] Collectively, these observations indicate that at least seven vibrational bands from the S_1 state of the Mn_4 cluster are observed in the NIR-excitation Raman spectrum of dark-adapted O_2-evolving PSII. The remainder of the Raman bands are due to PRR from Chl *a* in the PSII core complex.

One additional note concerns the Raman spectrum of illuminated O_2-evolving versus Mn-depleted PSII. In the spectrum of the former complex, a band occurs at 418 cm^{-1} that is not observed for the latter (or for dark-adapted O_2-evolving PSII). This feature is not readily apparent in the raw SERDS data (Figure 3); however, exclusion of a band in this region from the spectral reconstruction introduces a significant residual in this spectral region. It is possible that the 418 cm^{-1} band is a feature unique to the S_2 state of the Mn_4 cluster. On the other hand, it is also possible that it is due to Chl *a*. In this regard, the PRR spectrum of PSI exhibits a band at 413 cm^{-1} (Table 1).[33] However, it is not clear why the 418 cm^{-1} band would only be observed in the illuminated O_2-evolving sample and not in the dark-adapted or Mn-depleted samples.

Examination of Figure 10 (which compares the reconstructed low-frequency Raman spectra for dark-adapted O_2-evolving PSII in H_2O versus D_2O) reveals that the bands observed at 309, 348, 438, and 476 cm^{-1} in H_2O solutions are sensitive to D_2O/H_2O exchange. In D_2O solution, features are observed at 288, 342, 403, and 468 cm^{-1}. Significantly, all of the bands that are sensitive to D_2O exchange are bleached upon illumination and conversion from the S_1 to S_2 state of the Mn_4 cluster. The other three Raman bands associated with the S_1 state (377, 511, and 587 cm^{-1}) exhibit no discernible isotope shifts. The remaining Raman bands are also unaffected by D_2O exchange, which is consistent with their assignment as Chl *a* modes. [The small differences ($\leq$3 cm^{-1}) in the frequencies of certain bands attributed to Chl *a* are insignificant within experimental error.] The effects of D_2O/H_2O exchange on the low-frequency Raman bands attributed to the S_1 state of the Mn_4 cluster are summarized in Table 2. In constructing the table, it has been assumed that there is a one-to-one correspondence between the bands observed in the D_2O versus H_2O spectra. This correlation may not be appropriate as will be addressed in the Discussion Section.

Discussion

The NIR-excitation Raman studies reported herein establish that unique low-frequency vibrational signatures are observed from dark-adapted O_2-evolving PSII. The fact that these Raman bands bleach upon illumination, which converts the Mn_4 cluster from the S_1 to S_2 state, is further consistent with these modes originating from the S_1 state of the Mn_4 cluster. The observation of Raman scattering from the S_1 state rather than the S_2 state is unanticipated considering that the original impetus for the NIR-excitation Raman studies was to probe into the NIR absorption feature of the S_2 state that has been suggested by the NIR-excitation-induced photoconversion between the multiline and $g = 4.1$ forms of the S_2 state.[35,36] The fact that NIR-excitation Raman scattering from the S_1 state is observable above the background of strong PRR scattering from the Chl *a* pigments in the PSII core complex implies that a NIR absorption band is also present for the S_1 state of the Mn_4 cluster. Accordingly, the Raman scattering from the S_1 state gains intensity via resonance enhancement. On the basis of the rather limited excitation profile obtained for the RR bands of the S_1 state, the NIR absorption feature from this state appears to be centered near 820 nm. Oxo−manganese model complexes are known to have absorption bands in the NIR, and the NIR absorption of the di-μ-oxo dimanganese unit has been found to be composed of a superposition of several Mn d−d and oxo-to-Mn charge-transfer bands.[41] Because the OEC is known to contain di-μ-oxo dimanganese units, it is reasonable that an oxo-to-Mn charge-transfer transition would occur in the NIR and give rise to the observed resonance-enhanced Raman scattering from the S_1 state. The observation that the RR scattering from the S_1 state is relatively intense (compared with the low-frequency PRR scattering from Chl *a*, which is in fact quite weak), whereas that from the S_2 is negligible (or much weaker) further implies that (1) the NIR absorption band of the S_1 state is more intense near 820 nm than that of the latter, or (2) the RR scattering from the S_2 state is strongly damped (for example, via an ultrafast dephasing process), or both. Regardless, the fact that vibrational signatures are observed from the S_1 state affords the opportunity for a more detailed characterization of the structure of this state (and the OEC in general) than has been previously possible.

The elucidation of structure from the vibrational characteristics of the S_1 state of the Mn_4 cluster is contingent on the assignment of the various vibrational modes, and the detailed assignment of these modes requires a full complement of isotopic substitution data. The studies reported herein using D_2O/H_2O exchange provide an initial step toward this goal. The modes attributed to the S_1 state of the Mn_4 cluster all fall in the 300−600 cm^{-1} range. This spectral range generally encompasses that expected for metal−O (μ-oxo and carboxylate), metal−OH, metal−OH_2, and metal−Cl stretching vibrations plus the bending modes (rocking and wagging) of metal-bound H_2O. The exact frequencies for these types of vibrations when the metal is Mn will depend on the detailed structure of the complex. However, a survey of the vibrational assignments for several Mn model complexes provides some context for examining the S_1 state vibrational modes. These studies indicate the following frequency ranges for Mn−ligand modes: oxo-bridged $Mn_2(\mu\text{-}O)_2$ core vibrations, 600−700 cm^{-1}; Mn−O (carboxylate) stretches, 300−400 cm^{-1}; Mn−OH stretches, 400−500 cm^{-1}; Mn−OH_2 stretches, 300−400 cm^{-1}; and Mn−Cl stretches, 200−400 cm^{-1}.[23−25] Rocking, twisting, and wagging modes of Mn-coordinated water molecules are expected to occur in the 300−900 cm^{-1} region.[25] Theoretical considerations also suggest that di-μ-oxo and mono-μ-oxo bridges can be distinguished by their observed stretching frequencies.[53]

The fact that four of the seven S_1-state modes (309, 348, 438, and 476 cm^{-1}) exhibit sensitivity to D_2O/H_2O exchange clearly

(53) Dave, B. C.; Czernuszewicz, R. S. *Inorg. Chim. Acta* **1998**, *281*, 25−35.

suggests that the S_1 state of the Mn_4 cluster contains at least two H_2O or OH^- ligands. The lower limit of two H_2O or OH^- ligands is based on the fact that a single H_2O or OH^- ligand is not expected to give rise to four deuteriation sensitive modes in the 300−600 cm^{-1} region.[25] The observation of H_2O or OH^- bound to the S_1 state of the Mn_4 cluster is in agreement with previous spectroscopic studies. For example, EPR studies of the S_2 state, produced by low-temperature illumination when no ligand exchange occurs, provide evidence for direct ligation of H_2O to the S_1 state of the Mn_4 cluster.[13] In addition, inhibitor binding studies show that H_2O analogues such as amines[54] and alcohols[55] bind to the S_1 state. The binding of H_2O or OH^- to the Mn_4 cluster in the S_1 state has also been incorporated into a number of functional models for the OEC.[56−61] The structure of the S_3 state of the OEC from one of these models is shown in Figure 1. Although only one Mn-bound OH^- ligand is portrayed in Figure 1, there are clearly a number of potential H_2O/OH^- coordination sites on the Mn atoms in the cluster. Other models have two Mn-bound H_2O/OH^- ligands.[56,57,59] Indeed, rapid mass spectroscopic measurement of O_2 evolution from the OEC provide evidence for two substrate H_2O molecules bound to the S_3 state.[62] In addition, a μ-hydroxo ligand has been proposed as a ligand in the S_0 state[60] and could also be present in the S_1 state. These possibilities should be considered in light of the Raman data that indicate that the S_1 state of the Mn_4 cluster contains at least two H_2O or OH^- ligands.

The deuteriation-induced downshifts observed for the 309, 348, 438, and 476 cm^{-1} bands are 21, 6, 35, and 8 cm^{-1}, respectively (assuming a one-to-one correspondence between the bands observed in the D_2O versus H_2O spectra). The deuteriation-induced downshifts predicted for a Mn−OH versus $Mn-OH_2$ complex are summarized in Table 3. The predicted shifts were calculated with the simplest possible model, namely a diatomic, harmonic oscillator with the OH/OH_2 ligand treated as a point mass. This model is clearly an oversimplification, but more sophisticated treatments are not warranted in the absence of additional data. Inspection of Table 3 reveals that the observed deuteriation shifts for both the 348 and 476 cm^{-1} bands (6 and 8 cm^{-1}, respectively) closely match those predicted for bound OH^- (7 and 10 cm^{-1}, respectively). This agreement could be taken to indicate that the S_1 state of the Mn_4 cluster contains bound OH^- rather than bound H_2O ligands. However, bound H_2O cannot be excluded because the actual deuteriation shifts for a H_2O ligand of the Mn_4 cluster would be expected to be smaller than those predicted by the diatomic, harmonic oscillator model. Inspection of Table 3 also reveals that the observed deuteriation shifts for the 309 and 438 cm^{-1} modes are much larger than those predicted for either an OH^- or H_2O ligand using a simple diatomic, harmonic oscillator model. This observation further complicates the interpretation of the vibration characteristics of the S_1 state of the Mn_4 cluster. Clearly, additional studies with other isotopic labels are needed to elucidate fully the origin of the vibrational pattern observed for the S_1 state. These studies may also aid in determining the origin of the three remaining modes of the S_1 state which are deuteriation insensitive (587, 511, and 377 cm^{-1}). Possible assignments for these modes include vibrations of the oxo-bridged $Mn_2(\mu\text{-}O)_2$ core (587 and 511 cm^{-1}, although the frequencies are somewhat lower than those of model complexes) and Mn−O stretches of putative carboxylate ligands or Mn−Cl stretches (377 cm^{-1}). The absence of any appreciable deuteriation shifts for these Mn−ligand vibrations indicates that they are uncoupled from the $Mn-OH/OH_2$ vibrations.

Table 3. Calculated Deuteriation Shifts (cm^{-1}) for Mn−OH and $Mn-OH_2$ Stretching Modes[a]

	$\Delta(H_2O/D_2O)$		
mode	obs	calc(Mn−OH/OD)	calc($Mn-OH_2/OD_2$)
309	21	7	12
348	6	7	13
438	35	11	17
476	8	10	18

[a] Calculated assuming that $Mn-OH/OH_2$ is a diatomic, harmonic oscillator with the OH/OH_2 ligand treated as a point mass.

Future Perspectives. The studies reported herein indicate that NIR-excitation SERDS in combination with isotopic substitution has the potential to constrain a number of structural parameters of the OEC. For example, $^{18}O/^{16}O$ exchange could further characterize the $Mn-OH/OH_2$ modes assigned in this paper and potentially identify the Mn−O−Mn stretches as well. $^{15}N/^{14}N$ substitution might allow the assignment of Mn−N modes associated with the histidine ligand(s) of the Mn_4 cluster. $^{37}Cl/^{35}Cl$ and/or Ca/Sr substitution could assess the structural connection between the Mn_4 cluster and its cofactors. These isotopically/chemically exchanged PSII systems will be the focus of our future NIR-excitation RR studies of the OEC.

Acknowledgment. This work was supported by grants GM 39781 (D.F.B.) and GM 32715 (G.W.B.) from the National Institutes of Health, grant 96-35306-3398 (G.W.B.) from the National Research Initiative Competitive Grants Program/USDA, and a National Institutes of Health predoctoral traineeship, GM 08283 (D.H.S.).

JA9932885

(54) Beck, W. F.; Brudvig, G. W. *Biochemistry* **1986**, *25*, 6479−6486.
(55) Force, D. A.; Randall, D. W.; Lorigan, G. A.; Clemens, K. L.; Britt, R. D. *J. Am. Chem. Soc.* **1998**, *120*, 13321−13333.
(56) Hoganson, C. W.; Lydakis-Simantiris, N.; Tang, X.-S.; Tommos, C.; Warncke, K.; Babcock, G. T.; Diner, B. A.; McCracken, J.; Styring, D. *Photosynth. Res.* **1995**, *46*, 177−184.
(57) Hoganson, C. W.; Babcock, G. T. *Science* **1997**, *277*, 1953−1956.
(58) Pecoraro, V. L.; Baldwin, M. J.; Caudle, M. T.; Hsieh, W.-Y.; Law, N. A. *Pure Appl. Chem.* **1998**, *70*, 925−929.
(59) Tommos, C.; Babcock, G. T. *Acc. Chem. Res.* **1998**, *31*, 18−25.
(60) Limburg, J.; Szalai, V. A.; Brudvig, G. W. *J. Chem. Soc., Dalton Trans.* **1999**, 1353−1361.
(61) Siegbahn, P. E. M.; Crabtree, R. H. *J. Am. Chem. Soc.* **1999**, *121*, 117−127.
(62) (a) Messenger, J.; Badger, M.; Wydrzynski, T. *Proc. Natl. Acad. Sci. U.S.A.* **1995**, *92*, 3209−3213. (b) Hillier, W.; Messinger, J.; Wydrzynski, T. *Biochemistry* **1998**, *37*, 16908−16914.